Proceedings World Geothermal Congress 2020+1
Reykjavik, Iceland, April - October 2021

Thermoeconomic Comparison between ORC and Binary-flashing Cycle for Geothermal Energy

Lingbao Wang[a,b,c], Xianbiao Bu[a,b,c], Huashan Li[a,b,c],Yulie Gong[a,b,c,*]

[a] Guangzhou Institute of Energy Conversion, Chinese Academy of Sciences, Guangzhou 510640, China

[b] CAS Key Laboratory of Renewable Energy, Guangzhou 510640, China

[c] Guangdong Provincial Key Laboratory of New and Renewable Energy Research and Development, Guangzhou 510640, China

E-mail address: gongyl@ms.giec.ac.cn (YL Gong)

Keywords: Geothermal energy; Organic Rankine Cycle; Binary flashing cycle; Thermoeconomic; Payback period.

ABSTRACT

Geothermal energy has many advantages over other renewable energy, including weather-proof, great stability, high capacity factor, base-load abilities and less ecological effect. Nonetheless, geothermal energy presents its own particular challenges. The high initial investment and long payback time make the geothermal power generation lag behind wind and solar energy. The binary flashing cycle (BFC) system is supposed to be a promising technology for the recovery geothermal energy due to the full use of geofluid. The economic performance of the system still need to be evaluated. In this paper, the thermoeconomic comparison between ORC and binary-flashing cycle for geothermal energy has been investigated. R245fa is selected as the working fluid. With the thermal efficiency, exergy efficiency, net power output per unit geothermal brine mass flow rate, heat exchanger area and heat recovery efficiency as evaluation indexes, the flowsheet modeling and optimization in MATLAB simulation software were conducted. The simulation results reveal that the BFC system sacrifices efficiency, and acquires larger net power output. What is more, the preliminary discussion of the economic feasibility of BFC system applied in FengShun geothermal field is presented. It is indicated that the BFC system has obvious economic benefits, especially in non-flowing geothermal well.

1. INTRODUCTION

Nowadays, renewable energy resources have received enormous attention due to the increasing consumption of fossil fuels and massive discharge of pollutants. Among the renewable energies, geothermal is the most reliable and stable. There is a large potential and interest in using geothermal energy all over the world. However, water dominated low-grade geothermal heat resources below 150℃ account for 70% of the geothermal resources available all over the world [1]. Organic Rankine Cycle (ORC) is proved to be an efficient technology for the low temperature geothermal energy utilization, due to simple mechanism, low pressure requirement, compact and simple components, convenience of maintenance, and high recovery efficiency [2]. Extensive investigations have been carried out, including working fluid screening, system design and optimization [3-6].

Nevertheless, the thermal efficiency of the ORC is less than 12% generally, which is not as high as expected [7].The low efficiency limits the further application and development. It is not well-optimized in view of thermodynamics. The working fluid at the evaporator exist is saturated or superheated in the ORC. The latent heat of the evaporation heat is much larger than that of sensible heat, which is used for the temperature lift of the working fluid. As a consequence, the temperature and pressure of the vapor at the evaporator exit are relatively low attributing to the complete evaporation, which leads to lower power output. As a modification, the binary-flashing cycle (BFC) is proved to be an efficient technology to address such issue [8-14]. In the BFC, the working fluid is partly evaporated, lesser heat rate is demanded in the evaporation process. As a consequence, the evaporation temperature and pressure are higher than those in the ORC. The liquid working fluid from the evaporator is flashed to produce more steam at a lower temperature and then produces an extra work.

Recently, the research focusing on the BFC is very limited. Michaelides and Scott [8] studied the BFC driven by geothermal energy using freon, ammonia and isobutene as working fluids. It is demonstrated the BFC exhibited better thermodynamic performance with respect to the ORC. More than 20% work would be produced by the BFC. Shi and Miehaelides [9] investigated the BFC with dual flashing process employing ammonia, freon-12 and isobutene as working fluid, respectively. It is shown the BFC may produce up to 40% more power than an optimized conventional binary system. Yuan and Miehaelides [10] found the BFC may provide up to 25% more power than the ORC under the optimum design condition. The conclusion is consistent with that of Michaelides and Scott [8]. Edrisi and Michaelides [11] compared several pure working fluids, including normal butane, isobutane, hexane, pentane, refrigerant-114, and ammonia, for use in the BFC system. It is suggested that hexane and pentane appear to be better working fluids among the working fluids investigated. Michaelides [12] revealed that the overall entropy production is reduced in the BFC, which is regarded as future cycle for power generation from geothermal energy. Wang et al. [13] proposed the BFC with a regenerator to recover the waste heat of the expander exhaust. And the working fluid selection was also conducted. Wang et al. [14] compared the thermodynamic performance of the ORC, double-evaporator ORC and BFC. The evaluation indicators were thermal efficiency, power output per mass unit of geothermal brine, reinjection temperature of geothermal brine.

Previous studies of the BFC were focused on thermodynamic analysis and revealed the BFC outperform ORC from the viewpoints of thermodynamics. However, none of the previous investigation report the performance of BFC from the view in combination of thermodynamic performance and economic factors. To fill up this research gap, one of the objectives of the present study is the thermoeconomic comparison between the ORC and BFC for geothermal energy recovery. Furthermore, the preliminary economic feasibility of the BFC system applied in FengShun geothermal field is also discussed. Due to the excellent thermal performance and zero ozone depletion potential (ODP), R245fa is selected as the working fluid recommended by Ref. [15].The thermophysical properties is list in Table 1.

Table 1: Thermophysical Properties of R245fa

Fluid	Fluid type	Molecular mass (kg/kmol)	Critical temperature (°C)	Critical pressure (kPa)	Normal boiling point (°C)
R245fa	Dry	134.05	154.01	3651.00	15.14

2. SYSTEM MODELING

2.1 System Description

The principle of ORC is simple, as shown in Fig. 1, and the system description can be referred in Ref. [7]. The schematic diagram of the BFC is depicted in Fig. 2.The BFC mainly consists of two preheaters, a vapor generator, a separator, a high-pressure expander, a flash drum, a low-pressure expander a condenser, two working fluid pumps. The geothermal brine flows into the vapor generator and heats up the saturated liquid working fluid. The working fluid is in a two-phase state at the exit of the vapor generator. The mixture of liquid and vapor is sent to the separator, where the working fluid vapor is separated from the mixture and is fed to the high-pressure expander to produce work. The remaining liquid working fluid in the separator is sent to the flash drum, in which it is flashed at a lower temperature and pressure. An additional quantity of vapor is produced and fed to the low-pressure expand to produce more work. The remaining liquid working fluid released from the flash drum is pumped to preheater II and is heated by the geothermal brine from the vapor generator. The working fluid from the high-pressure and low-pressure expand is driven towards the condenser to be condensed to liquid state by rejecting heat to the cooling water. Subsequently, the working fluid is pumped to preheater I, where absorbs the heat of the geothermal brine from preheater II. Then the left geothermal brine is re-injected to the reservoir. Finally, the working fluid from preheater II is sent to vapor generator to continue cycle operation.

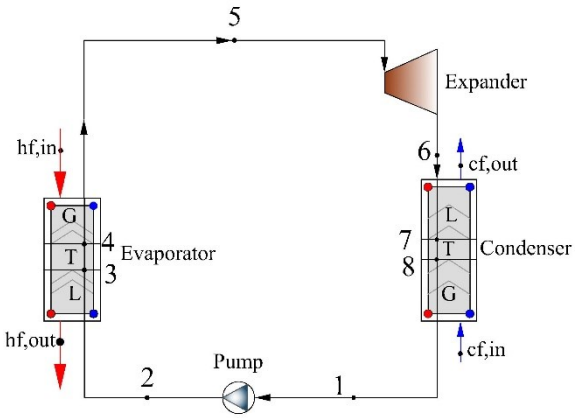

Figure 1: Schematic Diagram of the ORC

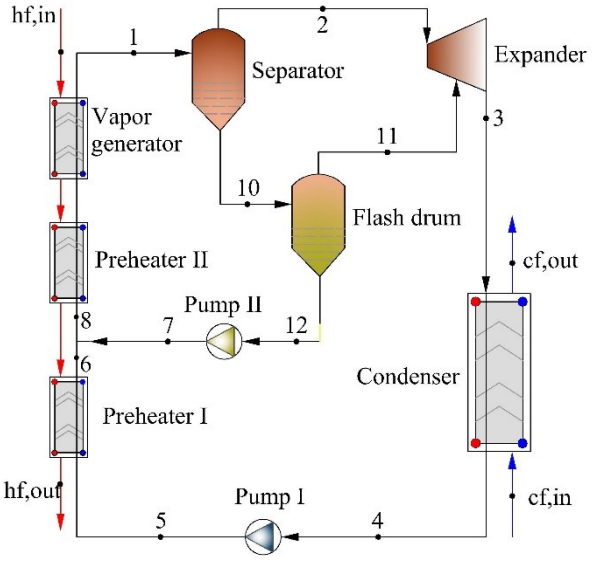

Figure 2: Schematic diagram of the BFC

2.2. Thermoeconomic Model

A steady state thermodynamic model of the BFC is developed, from which the thermodynamic model of ORC can be easily established. To simple the system model, several assumptions are listed as follows [16]:

(1) Pressure loss and heat dissipation of each component and the pipelines are negligible except for the turbine and pump;

(2) Friction losses, as well as the kinetic energy and potential energy of operating process are neglected;

(3) The working fluids at the condenser exit and expander inlet are supposed to be saturated state;

(4) The irreversibility related to the separator can be ignored;

(5) Counter-flow heat exchangers are adopted in this model;

(6) The geothermal brine has the properties of pure water;

(7) The pinch point temperature difference is set at 10 K and 5 K for the evaporator and condenser, respectively.

2.2.1 Thermodynamic Model

The plate heat exchanger is preferred, due to the advantages of compactness, high efficiency, easy maintenance, less fouling and flexibility [23]. The evaporator contains three components, i.e. preheater I, preheater II and vapor generator.

The saturated liquid mixtures enter into the vapor generator, and leave with a predetermined dryness fraction. The heat balance in the evaporator yields the following expression:

For the preheater I

$$Q_{\mathrm{Pre1}} = m_{\mathrm{hf}} c_{\mathrm{p,hf}} \left(T_{\mathrm{p,2}} - T_{\mathrm{hf,out}} \right) = m_5 \left(h_6 - h_5 \right) \tag{1}$$

$$m_5 = m_1 \left(qu_{\mathrm{gen}} + \left(1 - qu_{\mathrm{gen}} \right) qu_{\mathrm{fsh}} \right) \tag{2}$$

$$Q_{\mathrm{Pre2}} = m_{\mathrm{hf}} c_{\mathrm{p,hf}} \left(T_{\mathrm{p,1}} - T_{\mathrm{p,2}} \right) = m_{\mathrm{wf}} \left(h_9 - h_8 \right) \tag{3}$$

$$m_2 = m_1 qu_{\mathrm{gen}} \tag{4}$$

$$Q_{\mathrm{gen}} = m_{\mathrm{hf}} c_{\mathrm{p,hf}} \left(T_{\mathrm{hf,in}} - T_{\mathrm{p,1}} \right) = m_2 \left(h_1 - h_9 \right) \tag{5}$$

$$Q_{\mathrm{evp}} = Q_{\mathrm{Pre1}} + Q_{\mathrm{Pre2}} + Q_{\mathrm{gen}} \tag{6}$$

where Q is the heat transfer rate, kW; m is the mass flow rate, kg/s; c_{p} is the specific heat capacity, kJ/(kg·K); T is the temperature, $^{\mathrm{o}}$C; h is the specific enthalpy, kJ/kg; the subscripts "hf", "wf", "Pre1", "Pre2", "in", "gen" and "fsh" denote the heat source fluid, working fluid, preheater I, preheater II, vapor generator and flash drum, respectively; the subscripts "in" and "out" represent the inlet and exit, respectively. The subscript numbers of the equations presented in this section represent the working state points in the cycle, showing in Fig. 1.

For the separator

$$m_1 = m_2 + m_{10} \tag{7}$$

For the flash evaporator

$$m_{10} = m_{11} + m_{12} \tag{8}$$

$$m_{11} = m_{10} qu_{fsh} + m_{12} \tag{9}$$

where qu is the dryness degree of the working fluid.

For the high-pressure expander

The power output in the high-pressure expander is given by:

$$W_{\mathrm{exp}} = m_2 \left(h_2 - h_3 \right) + m_{11} \left(h_{11} - h_3 \right) = m_2 \left(h_2 - h_{2,\mathrm{s}} \right) \eta_{\mathrm{exp}} + m_{11} \left(h_{11} - h_{11,\mathrm{s}} \right) \eta_{\mathrm{exp}} \tag{10}$$

For the condenser

$$Q_{\text{con}} = m_{\text{cf}} c_{\text{p,cf}} \left(T_{\text{cf,out}} - T_{\text{cf,in}} \right) = m_3 \left(h_3 - h_4 \right) \tag{11}$$

$$m_3 = m_2 + m_{11} = m_{\text{wf}} q u_{\text{gen}} + m_{\text{wf}} \left(1 - x_{\text{gen}} \right) x_{\text{fsh}} \tag{12}$$

where the subscripts “con” and “cf” indicate the condenser and cooling water, respectively.

For the pump I

The power consumption of the pump I is expressed by:

$$W_{\text{pp1}} = m_5 \left(h_5 - h_4 \right) = m_5 \left(h_{4,\text{s}} - h_4 \right) / \eta_{\text{pp}} \tag{13}$$

$$m_5 = m_4 = m_3 \tag{14}$$

For the pump II

Similar to pump I, the power consumed by the pump II is calculated by:

$$W_{\text{pp2}} = m_{12} \left(h_7 - h_{12} \right) = m_{12} \left(h_{12,\text{s}} - h_{12} \right) / \eta_{\text{pp}} \tag{15}$$

where the subscript “pp” denotes the working fluid pump.

Then, the power output of the BFC can be calculated as follows:

$$W_{\text{net}} = W_{\text{exp}} - W_{\text{pp1}} - W_{\text{pp2}} \tag{16}$$

where the subscript “net” represents net power output.

The thermal efficiency is expressed by:

$$\eta_{\text{th}} = W_{\text{net}} / Q_{\text{tot}} \tag{17}$$

The second law efficiency is given by:

The input exergy of heat source fluid is defined as:

$$E_{\text{in}} = m_{\text{hf}} c_{\text{p,hf}} \left[\left(T_{\text{hf,in}} - T_{\text{hf,out}} \right) - T_0 \ln \left(\frac{T_{\text{hf,in}}}{T_{\text{hf,out}}} \right) \right] \tag{18}$$

Considering the inherent qualitative difference between heat and mechanical power, the second law analysis is applied as an additional tool to analyze the quality of energy or the potential of thermal energy to produce work. The exergy efficiency is defined as the ratio of the net output power to the total input exergy:

$$\eta_{\text{ex}} = W_{\text{net}} / E_{\text{in}} \tag{19}$$

The heat recovery rate is used to indicate the utilization degree of geothermal water, as given by:

$$UR = \frac{T_{hw,in} - T_{hw,out}}{T_{hw,in} - \left(\frac{m_5 T_5 + m_7 T_7}{m_5 + m_7} + pp_{eva} \right)} \tag{20}$$

where UR is the heat recovery rate; pp_{eva} is pinch point temperature difference, $^{\text{o}}$C.

2.2.2 Heat Exchanger Area Calculation

The evaporator contains three components, i.e. preheater I, preheater II and vapor generator. And the heat transfer area is calculated sectionalized.

The total heat transfer rate of each region is given by:

$$Q_{\mathrm{i}} = U_{\mathrm{i}} A_{\mathrm{i}} \Delta T_{\mathrm{m}} \tag{21}$$

where U_{i} is the overall heat transfer coefficient of each region, W/(m^2·K); A_{i} is the heat transfer area of each region, m^2; ΔT_{m} is the log mean temperature difference between the hot and cold fluid, K.

The log mean temperature difference is expressed by:

$$\Delta T_{\mathrm{m}} = \frac{\Delta T_{\max} - \Delta T_{\min}}{\ln\left(\Delta T_{\max} / \Delta T_{\min}\right)} \tag{22}$$

where $\Delta T_{\max}$ and $\Delta T_{\min}$ are maximum and minimum heat transfer temperature difference, respectively, K.

The overall heat transfer coefficient is given by:

$$\frac{1}{U_{\mathrm{i}}} = \frac{1}{\alpha_{\mathrm{i,hs}}} + \frac{\delta}{\lambda} + \frac{1}{\alpha_{\mathrm{i,cs}}} \tag{23}$$

where $\alpha_{\mathrm{i,hs}}$ is the heat transfer coefficient on the hot fluid side, W/(m^2·K). δ is the fin thickness, mm. λ is coefficient of thermal conductivity, W/(m·K). $\alpha_{\mathrm{i,cs}}$ is the heat transfer coefficient on the cold fluid side, W/(m^2·K).

The single-phase heat transfer coefficient in the evaporator is calculated using the correlation by Chisholm and Wanniarachchi [17].

$$Nu = \frac{\alpha_{\mathrm{i,hs/cs}} d_{\mathrm{h}}}{\lambda} = 0.724 \left(\frac{6\beta}{\pi}\right)^{0.646} Re^{0.583} Pr^{1/3} \tag{24}$$

where Nu is the Nusselt number; d_{h} is the hydraulic diameter, m; β is the corrugation angle on the surface of a plate; Re is the Reynolds number; Pr is Prandtl number.

$$Re = G d_h / \mu \tag{25}$$

where G is the mass velocity through the plate channels, kg/(m^2·s); μ is the viscosity, Pa·s.

$$Pr = \frac{C_p \eta}{\lambda} \tag{26}$$

The correlation proposed by Ref. [18] is employed to estimate the convection heat transfer coefficient on the cold side in the two-phase region of the evaporator.

$$Nu = \frac{\alpha_{\mathrm{i,cs}} d_{\mathrm{h}}}{\lambda} = 1.926\,\mathrm{Pr}^{1/3}\,\mathrm{Re}_{\mathrm{eq}}^{0.5}\,\mathrm{Bo}_{\mathrm{eq}}^{0.3} \left[1 - x_{\mathrm{m}} + x_{\mathrm{m}} \left(\frac{\rho_{\mathrm{l}}}{\rho_{\mathrm{v}}}\right)^{0.5}\right] \tag{27}$$

where Re_{eq} and Bo_{eq} are the equivalent Reynolds and boiling number; x_{m} is the vapor quality.

The heat released by the working fluid in the condenser is equal to the heat absorbed by the cooling water.

$$Q_{\mathrm{con}} = m_{\mathrm{cf}} c_{\mathrm{p,cf}} \left(T_{\mathrm{cf,out}} - T_{\mathrm{cf,in}}\right) = m_{\mathrm{wf}} \left(h_6 - h_1\right) \tag{28}$$

where the subscripts “con”, “cf” denote the condenser, cooling water, respectively.

The condenser is divided into three regions as well, i.e. a superheated region, a two-phase condensation region and supercooling region.

The single-phase heat transfer coefficient in the condenser is also calculated by Eq. (4).The convection heat transfer coefficient on the hot side in the two-phase region of the condenser is expressed as:

$$Nu = \frac{\alpha_{\mathrm{i,hs}} d_{\mathrm{h}}}{\lambda} = 4.118\,\mathrm{Re}^{0.4}\,\mathrm{Pr}^{1/3} \tag{29}$$

2.2.3 Economic Model

The cost of the heat exchangers is given by [19]:

$$C_{\mathrm{hx}}=\frac{CEPCI_{2017}}{CEPCI_{2001}}\times F_{\mathrm{s}}\times C_{\mathrm{hx}}^{0}\times\left(B_{1,\mathrm{hx}}+B_{2,\mathrm{hx}}\times F_{\mathrm{m,hx}}\times F_{\mathrm{p,hx}}\right) \tag{30}$$

where C_{hx} is the capitalized cost of the heat exchanger, USD; CEPCI_{2001} and CEPCI_{2017} are the Chemical Engineering Plant Cost Index for years 2001 and 2013; Fs is an additional factor for overhead cost; C_{hx}^{0} is the basic cost, USD; $B_{1,\mathrm{hx}}$， $B_{2,\mathrm{hx}}$ are the constants for the certain type of heat exchanger; $F_{\mathrm{m,hx}}$ is the material factor; $F_{\mathrm{p,hx}}$ is the pressure factor.

$$\log C_{\mathrm{hx}}^{0}=K_{1,\mathrm{hx}}+K_{2,\mathrm{hx}}\times(\log A_{\mathrm{hx}})+K_{3,\mathrm{hx}}\times(\log A_{\mathrm{hx}})^{2} \tag{31}$$

$$\log C_{\mathrm{hx}}^{0}=K_{1,\mathrm{hx}}+K_{2,\mathrm{hx}}\times(\log A_{\mathrm{hx}})+K_{3,\mathrm{hx}}\times(\log A_{\mathrm{hx}})^{2} \tag{32}$$

$$\log F_{\mathrm{p,hx}}=C_{1,\mathrm{hx}}+C_{2,\mathrm{hx}}\times(\log P_{\mathrm{hx}})+C_{3,\mathrm{hx}}\times(\log P_{\mathrm{hx}})^{2} \tag{33}$$

where $K_{1,\mathrm{hx}}$， $K_{2,\mathrm{hx}}$, $C_{1,\mathrm{hx}}$， $C_{2,\mathrm{hx}}$， $C_{3,\mathrm{hx}}$ are the constants; A_{hx} is heat exchanger area, m^2; P_{hx} is the pressure of heat exchanger, bar.

The cost of the working fluid pump is obtained by:

$$C_{\mathrm{pp}}=\frac{CEPCI_{2017}}{CEPCI_{2001}}\times F_{\mathrm{s}}\times C_{\mathrm{pp}}^{0}\times\left(B_{1,\mathrm{pp}}+B_{2,\mathrm{pp}}\times F_{\mathrm{m,pp}}\times F_{\mathrm{p,pp}}\right) \tag{34}$$

$$\log C_{\mathrm{pp}}^{0}=K_{1,\mathrm{pp}}+K_{2,\mathrm{pp}}\times(\log W_{\mathrm{pp}})+K_{3,\mathrm{pp}}\times(\log W_{\mathrm{pp}})^{2} \tag{35}$$

$$\log F_{\mathrm{p,pp}}=C_{1,\mathrm{pp}}+C_{2,\mathrm{pp}}\times(\log P_{\mathrm{pp}})+C_{3,\mathrm{pp}}\times(\log W_{\mathrm{pp}})^{2} \tag{36}$$

where C_{pp} is capitalized cost of the working fluid pump, USD; $F_{\mathrm{m,pp}}$ is an additional factor; $F_{\mathrm{p,pp}}$ is pressure factor; C_{pp}^{0} is the basic cost, USD; $B_{1,\mathrm{pp}}$, $B_{2,\mathrm{pp}}$, $K_{1,\mathrm{pp}}$, $K_{2,\mathrm{pp}}$， $K_{3,\mathrm{pp}}$, $C_{1,\mathrm{pp}}$, $C_{2,\mathrm{pp}}$, $C_{3,\mathrm{pp}}$ are the constants; P_{pp} is the pressure, bar; W_{pp} is the power consumption, kW.

The cost of the expander is given by:

$$C_{\mathrm{exp}}=\frac{CEPCI_{2017}}{CEPCI_{2001}}\times F_{\mathrm{s}}\times C_{\mathrm{exp}}^{0}\times F_{\mathrm{m,exp}} \tag{37}$$

$$\log C_{\mathrm{exp}}^{0}=K_{1,\mathrm{exp}}+K_{2,\mathrm{exp}}\times(\log W_{\mathrm{exp}})+K_{3,pp}\times(\log W_{\mathrm{exp}})^{2} \tag{38}$$

where C_{exp} is capitalized cost of the expander, USD; $F_{\mathrm{m,exp}}$ is pressure factor; C_{exp}^{0} is the basic cost; $K_{1,\mathrm{exp}}$, $K_{2,\mathrm{exp}}$, $K_{3,\mathrm{exp}}$ are the constants.

The parameters of the economic model are list in Table 2.

Table 2: Parameters of Economic Model [19-20]

Parameter	Value	Parameter	Value
CEPCI_{2001}	394	$F_{\mathrm{m,pp}}$	2.20
CEPCI_{2017}	623.5	$K_{1,\mathrm{pp}}$	3.389
F_{s}	1.70	$K_{2,\mathrm{pp}}$	0.536
$B_{1,\mathrm{hx}}$	0.96	$B_{1,\mathrm{pp}}$	1.89
$B_{2,\mathrm{hx}}$	1.21	$B_{2,\mathrm{pp}}$	1.35
$F_{\mathrm{m,hx}}$	2.40	$C_{1,\mathrm{pp}}$	-0.3935
$K_{1,\mathrm{hx}}$	4.66	$C_{2,\mathrm{pp}}$	0.3957
$K_{2,\mathrm{hx}}$	-0.1557	$C_{3,\mathrm{pp}}$	-0.00226
$K_{3,\mathrm{hx}}$	0.1547	$F_{\mathrm{m,exp}}$	3.50
$C_{1,\mathrm{hx}}$	0.00	$K_{1,\mathrm{exp}}$	2.2659
$C_{2,\mathrm{hx}}$	0.00	$K_{2,\mathrm{exp}}$	1.4398
$C_{3,\mathrm{hx}}$	0.00	$K_{3,\mathrm{exp}}$	-0.1776
		$K_{3,\mathrm{pp}}$	0.1538

The cost of separator and flashing tank can be estimated by [21]:

$$C_{\text{sep}}(C_{\text{fsh}}) = (2.25 + 1.82 \times 3.2) \times 10^{sf} \tag{39}$$

$$sf = 3.4974 + 0.4483 \log V + 0.1074 \log V \tag{40}$$

where V is the volume, m^3.

The cost of water pump is given by [22]:

$$C_{\text{watpp}} = 630 W_{\text{watpp}}^{\ 0.4} \tag{41}$$

$$W_{\text{watpp}} = m_{\text{wat}} g H_{\text{watpp}} / \left(1000 \eta_{\text{watpp}}\right) \tag{42}$$

where W_{watpp} is the mechanical power of the water pump, kW, kW; g is the acceleration of gravity, m/s^2; H_{watpp} is the hydraulic head, m; η_{watpp} is the efficiency of the water pump.

The total investment cost can be estimated by:

$$C_{\text{tot}} = C_{\text{hex}} + C_{\text{exp}} + C_{\text{pp}} + C_{\text{sep}} + C_{\text{fsh}} + C_{\text{watpp}} + C_{\text{well}} \tag{43}$$

where C_{well} is the mining rights cost, USD.

The operation and maintenance cost is given by [23]:

$$C_{\text{om}} = 6\% * C_{\text{tot}} \tag{44}$$

The operation cost of the water pump is given by:

$$C_{\text{OPR}} = W_{\text{watpp}} C_{\text{ele}} TPY \tag{45}$$

Where C_{ele} is unitary cost of the electricity, USD/kW; TPY is the annual operating time, h.

In consideration of time value of money, the payback period is calculated by:

$$W_{\text{net}} TPY C_{\text{ele}} - C_{\text{om}} - C_{\text{OPR}}\left(\left(1+\text{IntRate}\right)^{pb} - 1 / \left(\text{IntRate}\right)\right) = C_{\text{tot}} (1+\text{IntRate})^{(pb-1)} \tag{46}$$

where pb is payback period, year； TPY is annual operating time, year.

Based on the thermoeconomic model established, all codes were developed by MATLAB software. The properties of R245fa is referred to NIST REFPROP 9.0 [24]

3. MODEL VALIDATION

The thermal efficiency (η_{th}) and power output per ton of geothermal brine (PRW) against generation temperature (T_{gen}) are calculated by the present model and compared with the research conducted by Wang [14] under the same working condition with R245fa as working fluid. The comparison result is depicted in Fig. 3. The maximum deviations of η_{th} and PRW between the present solutions and results from Ref. [14] are less than 3.8% and 2.5%, respectively. It is indicated there is good agreement between the present work and Ref. [14]. That is to say the present model can be applied to predict the BFC system performance within the acceptable error range.

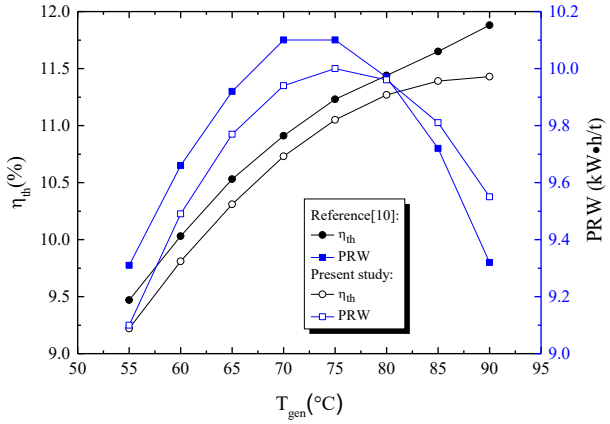

Figure 3: Validation of the Simulation Model

4. RESULTS AND DISCUSSION

4.1 Thermoeconomic Comparison between ORC and BFC

Based on the model developed above, the thermoeconomic comparison between ORC and BFC are conducted. The typical input parameters and boundary conditions under consideration are list in Table 3. Note that given efficiencies of expander and pump are significantly lower than those assumed in the literature [25-26], which is more realistic. The variations of W_{net} and A_{hex} for the ORC and BFC with generation pressure (P_{gen}) are displayed in Fig. 4. As can be seen, with the rising of P_{gen}, the W_{net} and A_{hex} of the ORC are decreased, while the W_{net} and A_{hex} of the BFC first increases and then decreases. The variation of W_{net} for the BFC is mainly due to that for a specific condensing temperature, an increase in P_{gen} leads to the specific enthalpy drop in the expander increasing, but meanwhile it will decrease the mass rate of working fluid. With the interaction between these two effects, an optimum P_{gen} occurs and makes W_{net} maximized, which is well in conformity with Ref. [11]. The optimal P_{gen} is 870 kPa, at which W_{net} and A_{hex} achieve the maximum. As can be seen the W_{net} and A_{hex} of the BFC are always higher than those of the ORC. With the rising of P_{gen}, the ratio of W_{net} of the BFC to that of the ORC increases basically linearly. The W_{net} of the BFC is 32 percent larger than that of the ORC with P_{gen} of 1400 kPa. Nevertheless, the ratio of A_{hex} of the BFC to that of the ORC first rises then declines, after reaching the peak value (1.8) at 870 kPa. To sum up, the BFC produces more work compared with the ORC. In the meantime, the heat exchangers investment cost of the BFC is much larger.

Table 3: Input Parameters of Simulation Calculation

Parameters	Value
Inlet temperature of geothermal brine (°C)	120°C
Mass flow rate of geothermal brine（kg/s）	1.0
Inlet temperature of cooling water (°C)	20°C
Efficiency of expander	0.65
Efficiency of work fluid pump	0.5
Ambient temperature (°C)	20°C
Generation pressure（kPa）	1000
Dryness degree	0.3
Condensation temperature (°C)	30°C
Flashing temperature (°C)	（T_{eva}+T_{con}）/2
Plate thickness (mm)	0.6
Plate spacing (mm)	2
Corrugation pitch (mm)	7.2
Chevron angle（°）	45

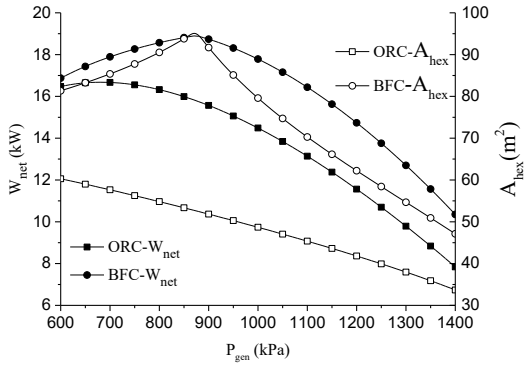

Figure 4: Variations of W_{net} and A_{hex} for the ORC and BFC with P_{gen}

The variations of η_{th} and η_{ex} for the ORC and BFC with P_{gen} are depicted in Fig. 5. As expected the η_{th} of the ORC and BFC increase with the rising P_{gen}, presenting the same behavior. The η_{ex} of the ORC is increased as P_{gen} increases. While the η_{ex} of the BFC first rises and subsequently decreases, there exists an optimum P_{gen} of 950 kPa, at which the η_{ex} obtains the maximum. The dryness degree of the working fluid at the evaporator exist is fixed constant in the present study. The heat transfer temperature difference between the working fluid and the geofluid is decreased with the increasing P_{gen}, leading to the rising of the reinjection temperature of geofluid. As a consequence, the input exergy is decreased. The variation of W_{net} has already shown in Fig. 4. With the interaction between the two effects, an optimum P_{gen} exists and makes the η_{ex} obtain the maximum value. It is obvious that the η_{th} and η_{ex} of the ORC are higher than those of the BFC. When P_{gen} is 1100 kPa, the η_{th} and η_{ex} of the ORC are 1.26 and 1.14 times as large as those of the BFC.

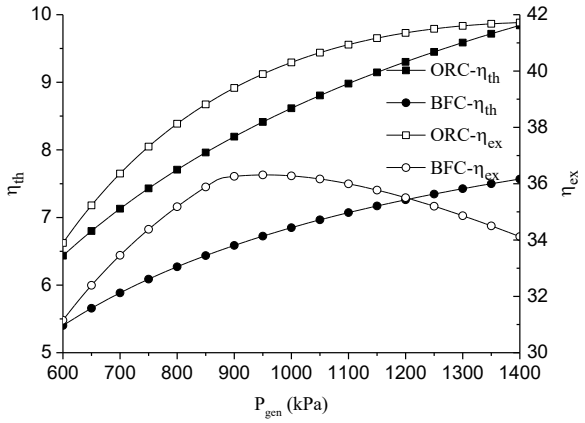

Figure 5: Variations of η_{th} and η_{ex} for the ORC and BFC with P_{gen}

The heat recovery efficiency is an important indicator for the low-grade waste heat utilization. For the non-flowing geothermal energy, the acquiring of geothermal water will require power consumption for the hot water pump. To make full use of the geothermal water is beneficial for the system. It is of practical significance to evaluate the system performance with the heat recovery efficiency as criteria. The variations of $T_{th,out}$ and UR for the ORC and BFC with P_{gen} are depicted in Fig. 6. As can be discovered, the $T_{th,out}$ of the BFC is 15-20 °C lower than that of ORC. And the UR of BFC is always much larger than that of ORC. The UR of BFC is 1.96 times as much as that of ORC. After comprehensive consideration, the BFC system obtains the larger net power output, sacrificing its efficiency.

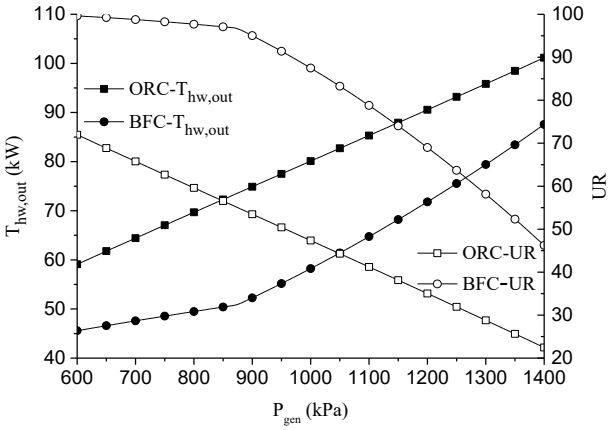

Figure 6: Variations of $T_{th,out}$ and UR for the ORC and BFC with P_{gen}

4.2 Case Study of the ORC and BFC in Fengshun Geothermal Plant

The first geothermal power generation station with capacity of 300 kW was established in 1970 in Dengwu village of Fengshun county, Guangdong province, which marked that China became the eighth country using geothermal energy for power generation in the world. The geothermal well is 800 m deep and supplies water at 91 °C. The geothermal water is pumped to the flashing tank from the well with the mass flow rate of 63.4kg/s. The water from the river nearby is used to cooling the turbine exhaust. The power station had retired since the last year and finished the historical mission. From the above-mentioned investigation, the BFC has the advantage of higher utilization rate of geothermal water compared with the ORC due to lower reinjection temperature. The preliminary economic feasibility study of BFC will be investigated based on working condition in Fengshun. The input parameters of the economic simulation are listed in Table 4. The economic comparison of the ORC and BFC is presented in Table 5. As can be seen, the total investment cost, maintenance cost and electric charge of water pump for the BFC are all higher than those of the ORC. Meanwhile, with the P_{gen} of 600, 700 and 740 kPa, the W_{net} of the BFC is 1.26, 1.41 and 1.68 times as large as those of ORC, and compared with the ORC, the payback period of the BFC is shortened by 1.9, 3.5 and 7.4 years, respectively. The payback period of BFC is just 6.0 years under the P_{gen} of 600 kPa. It is indicated that the BFC exhibits better economic benefits.

Table 4: Input Parameters of Economic Simulation

Parameter	Value
Inlet temperature of geothermal water (°C)	91
Mass flow rate of geothermal water (kg/s)	63.4
Inlet temperature of cooling water (°C)	14.4
Condensation temperature (°C)	30
Efficiency of expander	0.65
Efficiency of working fluid pump	0.5
Efficiency of water pump	0.8
Interest rate	0.1
Annual operation time (h)	8000
Life time (year)	30

Table 5: Economic Comparison of the ORC and BFC

Parameters	ORC			BFC		
Generation pressure (kPa)	660	700	740	660	700	740
Condensation temperature (°C)	30	30	30	30	30	30
Pinch point temperature difference (°C)	5	5	5	5	5	5
mining rights cost (million yuan)	8	8	8	8	8	8
Total investment cost (million yuan)	1.55	1.53	1.50	2.12	2.36	2.93
Maintenance cost (thousand yuan)	93	92	90	127	141	176
Electric charge of water pump (million yuan)	0.29	0.28	0.28	0.32	0.32	0.33
Net power output (kW)	372	328	281	470	461	473
Power output per unit geothermal water (kWh/t)	1.63	1.44	1.23	2.06	2.02	2.07
Payback period (year)	7.9	10.0	14.3	6.0	6.5	6.9

5. CONCLUSIONS

In the present paper, the thermoeconomic comparison between the ORC and BFC for geothermal energy is conducted. The main contribution is the contrast from the viewpoint of economic and the preliminary discussion of the economic feasibility of BFC system applying in FengShun geothermal field. According to the investigation, several conclusions can be drawn as following:

(1) With the rising P_{gen}, the W_{net} and A_{hex} of the ORC are decreased, while the W_{net} and A_{hex} of the BFC first increase, and then decrease after reaching the peak point at 870 kPa. The W_{net} and A_{hex} of the BFC are always higher than those of the ORC.

(2) The η_{ex} of the BFC first rises and subsequently declines, the optimum P_{gen} is 950 kPa. The η_{th} and η_{ex} of the ORC are higher than those of the BFC. The η_{th} and η_{ex} of the ORC are 1.26 and 1.14 times as large as those of the BFC, with the P_{gen} of 1100 kPa.

(3) The $T_{th,out}$ of the BFC is much lower than that of the ORC, approximately 15-20°C. The *UR* of the BFC is always much larger than that of the ORC. The *UR* of BFC is 1.96 times as much as that of the ORC. After comprehensive consideration, the BFC obtains the larger net power output, sacrificing its efficiency.

(4) The total investment cost, maintenance cost and electric charge of water pump for the BFC are all higher than those of the ORC. In the meantime, with the P_{gen} of 600, 700 and 740 kPa, the W_{net} of the BFC is 1.26, 1.41 and 1.68 times as large as those of the ORC, and compared with the ORC, the payback period of the BFC is shortened by 1.9, 3.5 and 7.4 years, respectively. The payback period of BFC is only 6.0 years under the P_{gen} of 600 kPa. It is indicated that the BFC exhibits excellent economic benefits, especially in non-flowing geothermal well.

6. ACKNOWLEDGEMENTS

The authors gratefully acknowledge the financial supports provided by the National Key Research and Development Program of China (No. 2018YFB1501805), and Natural Science Foundation of Guangdong Province (No. 2018A030313018), and the Youth Innovation Promotion Association, Chinese Academy of Sciences (No. 2017402).

REFERENCES

[1] Franco, A., and Vaccaro, M.: Numerical simulation of geothermal reservoirs for the sustainable design of energy plants: a review, Renewable and Sustainable Energy Reviews, **30**, (2014), 987-1002.

[2] Cao, Y., and Dai Y.P.: Comparative analysis on off-design performance of a gas turbine and ORC combined cycle under different operation approaches, Energy Conversion and Management, **135**, (2017), 135, 84-100.

[3] Rayegan, R., and Tao, Y.X.: A procedure to select working fluids for Solar Organic Rankine Cycles (ORCs), Renewable Energy, **36**, (2011), 659-670.

[4] Astolfi, M., Romano, M.C., Bombarda, P., Macchi, E.: Binary ORC (Organic Rankine Cycles) power plants for the exploitation of medium-low temperature geothermal sources- Part B: Techno-economic optimization, Energy, **66**, (2014), 435-446.

[5] Li, T.L., Yuan, Z.H., Li, W., Yang, J.L., Zhu, J.L.: Strgenthening mechanisms of two-stage evaporation strategy on system performance for organic Rankine cycle, Energy, **101**, (2016), 532-540

[6] Miao, Z., Xu, J.L., Zhang, L.: Experimental and modeling investigation of an organic Rankine cycle system based on the scroll expander, Energy, **134**, (2017), 35-49.

[7] Basaran, A., and Ozgerer, L.: Investigation of the effect of different refrigerants on performances of binary geothermal power plants, Energy Conversion and Management, **76**, (2013), 483-498.

[8] Michaelides, E.E., and Scott, G.J.: A binary-flashing geothermal power plant, Energy, **9**, (1984), 323-331.

[9] Shi, H., and Michaelides, E.E.: Binary dual-flashing geothermal power plants, International Journal of Energy Research, **13**, (1989), 127-135.

[10] Yuan, Z., and Michaelides, E.E.: Binary-flashing geothermal power plants, Journal of Energy Resources Technology, **115**, (1993), 232-236.

[11] Edrisi, B.H., and Michaelides, E.E.: Effect of the working fluid on the optimum work of binary-flashing geothermal power plants, Energy, **50**, (2013), 389-394.

[12] Michaelides, E.E.: Future directions and cycles for electricity production from geothermal resources, Energy Conversion and Management, **107**, (2016), 3-9.

[13] Wang, L.B., Bu, X.B., Li, H.S., Wang, H.Z., Ma, W.B.: Working fluids selection for flashing organic rankine regeneration cycle driven by low-medium heat source, Environmental Progress and Sustainable Energy, **37**, (2018), 1201-1209.

[14] Wang, Y.X., Wang, L.B., Li, H.S., Bu, X.B.: Thermodynamic calculation and optimization of geothermal power generation in Ganzi, Journal of Harbin Engineering University, **37**, (2016), 873-877.

[15] Rayegan, R., and Tao Y.X.: A procedure to select working fluids for Solar Organic Rankine Cycles (ORCs), Renewable Energy, **36**, (2011), 659-670.

[16] Van, L.L., Michel, F., Abdelhamid, K., Sandrine, P.P.: Performance optimization of low-temperature power generation by supercritical ORCs (organic Rankine cycles) using low GWP (global warming potential) working fluids, Energy, **67**, (2014), 513-526.

[17]Chisholm, D., Wanniarachchi, A.S.: Maldistribution in single-pass mixed- channel plate heat exchangers, Compact Heat Exchangers for Power and Process Industries, HTD-ASME, **201**, (1992), 95-99.

[18]Yan, Y.Y., and Lin, T.F.: Evaporation Heat Transfer and Pressure Drop of Refrigerant R-134a in a Plate Heat Exchanger, Journal of Heat Transfer, **121**, (1999), 118-127.

[19] Hou, S.Y., Zhou, Y.D., Yu, L.J., Zhang, F.Y., Cao, S.: Optimization of the combined supercritical CO_2 cycle and organic Rankine cycle using zeotropic mixtures for gas turbine waste heat recovery, Energy Conversion and Management, **160**, (2018), 313-325

[20]Imran, M., Park, B.S., Kim, H.J., Lee D.H., Usman, M., Heo, M.: Thermo-economic optimization of Regenerative Organic Rankine Cycle for waste heat recovery applications, Energy Conversion and Management, **87**, (2014), 107-118.

[21] Zhao, Y.J., and Wang, J.F.: Exergoeconomic analysis and optimization of a flash-binary geothermal power system, Applied Energy, **179**, (2016), 159-170.

[22]Berhane, H.G., Gonzalo, G.G., Laureano, J., Dieter, B.: Design of environmentally conscious absorption cooling systems via multi-objective optimization and life cycle assessment, Applied Energy, **86**, (2009), 1712-1722.

[23] Mosaffa, G. F., Mosaffa, A.H., Farshi, L.G.: Exergoeconomic and environmental analyses of an air conditioning system using thermal energy storage, Applied Energy, **162**, (2016), 515-526.

[24] Lemmon, E.W., Huber, M.H., McLinden, M.O.: REFPROP, NIST Standard Reference Database 23 (2013) Version 9.1, USA.

[25] Yang, M.H., Yeh, R.H., Hung, T.C.: Thermo-economic analysis of the transcritical organic Rankine cycle using R1234yf/R32 mixtures as the working fluids for low-grade waste heat recovery, Energy, **140**, (2017), 818-836.

[26] Meng, F.X., Zhang, H.G., Yang, F.B., Hou, X.C., Lei, B., Zhang, L., Wu, Y.T., Wang, J.F., Shi, Z.C.: Study of efficiency of a multistage centrifugal pump used in engine waste heat recovery application, Applied Thermal Engineering, **110**, (2017), 779-786